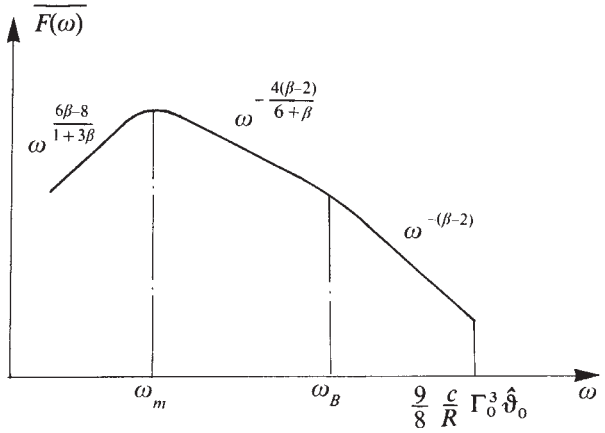

Fig. 1 The curvature radiation spectrum for $\vartheta_{\Omega B} \sim 1$, $\vartheta_K^{\min} = 0$ and $\beta > 2$.

bunches $\dot{N}_B$ from a pulsar should be used, rather than e, m and $\dot{N}$. The quantities are related as $Q = |n_+ - n_-|e = \zeta ne$, $M = nm$ and $\dot{N}_B = \dot{N}/n$, where n_+ and n_- are the number of positrons and electrons in a bunch, respectively; $n = n_+ + n_-$, $\zeta = |n_+ - n_-|/n$ is the degree of charge separation in the bunches of ejected plasma. Substituting Q, M and $\dot{N}_B$ in equations (5) and (6) shows clearly that ω_m and ω_B do not depend on n; there is, however, a relatively weak dependence of ω_m and ω_B on $\zeta(\omega_m, \omega_B \propto \zeta^{2/(2+\beta)})$. If the number of particles n in a bunch is changing, the radiation spectrum (see Fig. 1) shifts along the $\overline{F(\omega)}$ axis ($\overline{F(\omega)} \propto n$ at $\zeta =$ constant), although it does not change its shape.

Table 1 summarizes the α values of the curvature radiation flux as a function of frequency dependence ($\overline{F(\omega)} \propto \omega^{-\alpha}$) for different frequency ranges, with β equal to 3, 4 or 5; ω_m and ω_B frequency values are also given for most probable parameters of pulsars[8-10,12]: $\dot{N} = 10^{33}$ particles $\times s^{-1}$, $R = 1.4 \times 10^6$ cm, $\Gamma_0 = 800$, $\hat{\vartheta}_0 = 10^{-2}$ and with ζ assumed equal to 0.1. In this case, whatever, the value of β, the radiation spectrum extends to the frequency $(9/8)(c/R)\Gamma_0^3\hat{\vartheta}_0$, which is $\sim 1.7 \times 10^{11}$ Hz.

The following are the main observational data about low-frequency cutoffs in the pulsar radio emission spectra (for details see ref. 7). (1) The mean frequency of the pulsar radio emission maximum below which the radio emission flux decreases ($\alpha < 0$), is $\omega_m = 130 \pm 80$ MHz. (2) The mean value of the radio emission spectral index in the frequency range below the maximum ($\omega < \omega_m$) is -1.4 ± 0.4. (3) The spectral indices of pulsar radio emission at frequencies higher or lower than the maximum frequency are almost equal in absolute magnitude and opposite in sign, that is, the steeper the radio emission spectrum up to its maximum ($\omega < \omega_m$), the steeper it is after it ($\omega > \omega_m$).

Table 1 shows that when $\beta = 4 \pm 1$ there is a good agreement between the expected behaviour of the curvature radiation spectrum, near its maximum, and the observational data. The ω_m versus β dependence is rather weak.

Above we have considered the case $\vartheta_K^{\min} = 0$, when in the pulsar rotation process its magnetic axis may coincide with the direction towards the observer. With the results from ref. 11 it is easily shown that the ω_m frequency value and the curvature radiation spectrum behaviour near the maximum at $\vartheta_K^{\min} \neq 0$ do not differ essentially from the case of $\vartheta_K^{\min} = 0$ if

$$\vartheta_K^{\min} < \vartheta_r \equiv \frac{8}{9}\frac{R}{c}\frac{\omega_m}{\Gamma_0^3}\hat{\vartheta}_0^{-2} \qquad (7)$$

At $\omega_m = 130$ MHz, $R = 1.4 \times 10^6$ cm, $\Gamma_0 = 800$ and $\hat{\vartheta}_0 = 10^{-2}$, we have $\vartheta_r \simeq 0.1$, that is, the ϑ_r value is sufficiently large ($\vartheta_r \gg \hat{\vartheta}_0$); hence for most pulsars $\vartheta_K^{\min} = 0$ may be assumed when the curvature radiation spectrum is considered to be near its maximum.

Note that the model presented here for the generation of pulsar radio emission due to the curvature mechanism may also explain the radio emission spectrum behaviour at higher frequencies (see Fig. 1). Thus, the ω_B frequency (several GHz, see Table 1) falls into the interval of the observed values of the higher-frequency break of the pulsar radio emission spectrum[1,7]. The observed values of the spectral indices after the high-frequency break are ~2 to 3 (refs 1, 7, 8), which corresponds to $(\beta - 2)$ for the same values $\beta \simeq 4$–5.

Received 4 January; accepted 22 February 1984.

1. Sieber, W. *Astr. Astrophys.* **28,** 237–252 (1973).
2. Kuzmin, A. D. *et al. Mon. Not. R. astr. Soc.* **185,** 441–449 (1978).
3. Bruck, Yu. M. *et al. Sov. astr. J.* **55,** 1031–1039 (1978).
4. Izvekova, V. A., Kuzmin, A. D., Malofeev, V. M. & Shitov, Yu. P. *Sov. astr. J.* **56,** 322–337 (1979).
5. Izvekova, V. A., Kuzmin, A. D., Malofeev, V. M. & Shitov, Yu. P. *Aust. J. Phys.* **32,** 25–38 (1979).
6. Malofeev, V. M. & Malov, I. F. *Sov. astr. J.* **57,** 90–106 (1980).
7. Izvekova, V. A., Kuzmin, A. D., Malofeev, V. M. & Shitov, Yu. P. *Astrophys. Space Sci.* **78,** 45–72 (1981).
8. Manchester, R. N. & Taylor, J. H. *Pulsars* (Freeman, San Francisco, 1977).
9. Sturrock, P. A. *Astrophys. J.* **164,** 529–556 (1971).
10. Ruderman, M. & Sutherland, P. *Astrophys. J.* **196,** 51–72 (1975).
11. Ochelkov, Yu. P. & Usov, V. V. *Astrophys. Space Sci.* **69,** 439–460 (1980).
12. Arons, J. *Proc. IAU Symp.* No. 94, 175–203 (1981).

Structure, stability and evolution of Saturn's rings

Frank G. Bridges*, A. Hatzes† & D. N. C. Lin†

* Board of Studies in Physics, and † Lick Observatory and Board of Studies in Astronomy and Astrophysics, University of California, Santa Cruz, California 95064, USA

Recent data obtained from the Voyager spacecrafts and ground-based measurements indicate: (1) the rings have a thickness of at most 150 m (ref. 1) and probably several times less[2,3]; (2) the rings are mostly composed of ice particles ranging from centimetres to metres in size[4]; (3) the rings are subdivided into a large number of ringlets with a radial dimension ranging from 10-km down to the several metres resolution of the Voyager spacecraft's camera[5]; (4) the B ring contains very many optical depth variations (0.6–3)[3]. This behaviour is essentially determined by the collisional properties of the rings' ice particles. Here we report some preliminary results from an experiment designed to measure the coefficient of restitution of ice particles colliding at impact velocities relevant to Saturn's rings. We apply these results to simple dynamical models for Saturn's rings and deduce the rings' thickness to be <5 m. We also show that regions with optical depth <0.5, such as the B ring, are unstable to viscous diffusion. Such an instability may be the cause of optical depth variations in the B ring.

The global properties such as the ring thickness and dynamical evolution time scale are basically determined by the collisional dynamics between the ring constituents and the resultant transport processes[6–9]. The cumulative effect of many collisions over a differentially rotating disk, such as Saturn's rings, is to establish a viscous stress which induces an outward transfer of angular momentum, an inward diffusion of mass[10], and an energy transfer from systematic shear into dispersive motion at a rate $\dot{E}_t \approx \upsilon\Sigma\Omega^2 r^2$, where Ω and Σ are respectively the angular frequency and surface mass density of the disk at radius r. The kinematic viscosity of the disk, is defined by $\upsilon \approx \sigma^2/[\Omega(\tau + \tau^{-1})]$ where $\tau = \Sigma A/m$ is the optical depth, A is the cross-section, m the mass of a typical ring particle, and σ is the average amplitude of the velocity dispersion. The particle collisions are partially inelastic and dissipate the kinetic energy associated with dispersive motion at a rate $\dot{E}_d \approx (1 - \varepsilon^2) r^2 \omega_c \Sigma \sigma^2$ where ε is the coefficient of restitution. The collision frequency, ω_c, is related to Ω such that $\omega_c = \tau\Omega$. A local energy equilibrium is established when $\dot{E}_t = \dot{E}_d$, that is,

$$(1 - \varepsilon^2)(1 + \tau^2) \approx b \qquad (1)$$

where b is of the order of unity. Assuming that the rings are

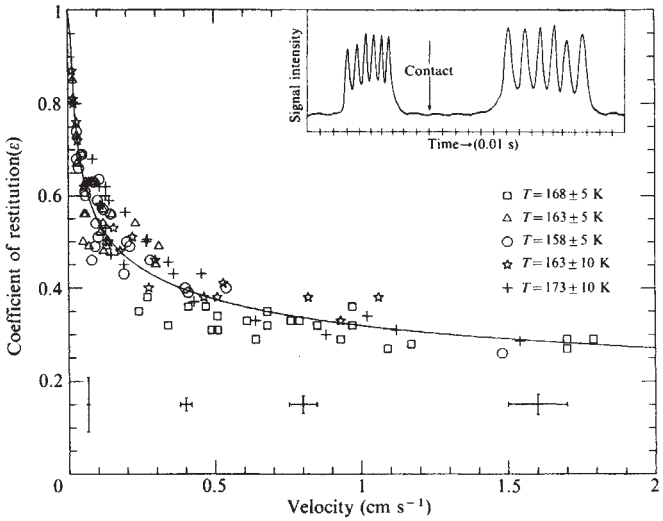

Fig. 1 A plot of the coefficient of restitution as a function of impact velocity for measurements at several different temperatures over the range 158–173 K. Estimates of the typical error bars are shown for four velocities at the bottom. The inset shows two sets of pulses obtained immediately before and after a collision. The values of ε and the velocity are obtained from the spacings of these pulses.

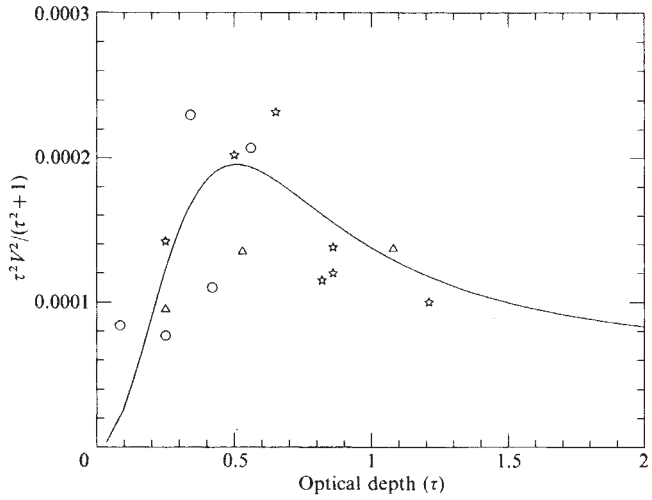

Fig. 2 A plot of $\tau^2V^2/(\tau^2+1)$ as a function of optical depth τ. The values for τ were obtained using equation (1). The points are obtained from the data in Fig. 1 and the solid line is a graph of $\tau^2V^2/(\tau^2+1)$ versus τ according to equation (4).

made of non-rotating, indestructable, and identical size ice spheres with a gaussian phase space distribution, b is determined from the rigorous treatment of the collisional Boltzmann equation[8]. An approximate analytical fit of these results indicates $b \approx 0.61$.

For most solid substances, ε is a function of the impact velocity, V (ref. 11). If an ε–V (or equivalently ε–σ) relationship is available, it can be applied to equation (1) to deduce a τ–σ relationship. If a disk is made up of nearly equally sized particles, its r.m.s. thickness, H, would be $\sim 2f\sigma/\Omega$. Here f is introduced to account for the anisotropy of the velocity dispersion ellipsoid and is of the order of unity ($f \to 1/\sqrt{6}$ as $\tau \to \infty$)[8,12]. Thus, an accurately determined ε–V relationship can be used to deduce H directly.

Another reason for determining an ε–V relation is associated with the viscous stability of disk flow. Several authors[13–15] have suggested that the condition for thermal and viscous stability cannot be satisfied simultaneously if $\tau \gg 1$. In these conditions the rings have a tendency to break up into many ringlets. This mechanism seems to offer a viable explanation for the origin of the density variations in the optically thick B ring where tidal effects due to various saturnian satellites are negligibly small. Physically, if the viscous couple, $W = 3\pi\Omega r^2 \Sigma v$, increases with τ, the rings are stable whereas if W decreases with τ the rings are unstable. The W–τ relationship can also be derived from an ε–V relationship. We have designed an experiment and determined this ε–V relationship in a laboratory environment.

To measure ε for ice particles in the conditions assumed to exist in Saturn's rings, the apparatus must meet several criteria. First, the relevant impact velocity must be in the range 0.01–5 cm s^{-1}. Second, the frictional damping of the system must be small compared with the kinetic energy associated with ice particle collisions such that the damping correction factor is relatively small. Third, the relevant ambient temperature should be in the range 100–150 K. Fourth, before and after each collision, the ice particles must be separated by a sufficiently large distance, say >0.01 cm, such that tiny powdered ice chips on their surface do not induce strong interactions between them except during the course of each collision. Finally the collisions should resemble free collisions as closely as possible.

The simplest experimental system which can satisfy most of the above requirements is to attach an ice ball to an oscillator and let it strike a stationary block of ice. A sufficiently low impact velocity and a reasonably large oscillator amplitude can be achieved with a compound pendulum with the axis of rotation very close to the centre of mass. In this case, the angular frequency is $(Mgd/I)^{1/2}$ where M and I are the mass and moment of inertia of the system. We constructed such a system using a disk mounted on an aluminium rod. Small weights at the top and bottom of the disk allow us to adjust the distance between the centre of mass and the suspension (that is rotation) axis, d. An ice ball is attached to one edge of the disk and a counter weight on the other edge in a manner such that their centre of mass is at the centre of the disk. The entire system is suspended by knife blades resting on polished agate plates. With this system, we have achieved periods as long as 60 s with the Q-value equal to 4. For shorter oscillation periods, such as $T < 30$ s, $10 < Q < 30$.

The main limitation of the above system is that collisions are not entirely free. The coupling between the ice particles and the pendulum body will cause a slight elastic deformation in the pendulum during a collision. However, we note that most of the kinetic energy dissipation occurs as a result of fracturing at the tiny contact surface area of the ice particles. For typical impact velocities the time interval during contact is considerably longer than the sound crossing time across the ice balls. Our experiments indicate that a sufficiently rigid mounting of the ice particle onto the pendulum effectively eliminated temporary redistribution of elastic energy within the system and thereby provided a good measure of ε.

The ambient temperature of the system is set at 150–175 K using a simple cryostat constructed from styrofoam and cooled with liquid nitrogen. The ice-block temperature is measured with an Omega thermocouple thermometer frozen into the ice block. The velocity of the ice ball is measured by reflecting a laser beam off a mirror mounted on the rotation axis of the pendulum. The reflected beam passes over a photocell masked with five slits 1 mm wide, 2 mm apart and situated 4 m from the pendulum. The photocell is positioned close to the point which corresponds to contact. Five pulses produced immediately before and after each collision provide an accurate measurement of the incoming and outgoing velocities from which ε can be deduced. Five slits are used primarily to improve the accuracy of the measurement and to eliminate damping contributions associated with the finite Q value of the pendulum. The results of our experiments indicate that only a small, that is <2%, correction is ever needed to account for damping.

A typical pulse train and the summary of the results obtained from the four lowest temperature runs are illustrated in Fig. 1. The general behaviour of ε as a function V is typical of the data taken at other temperature ranges. The data can be qualitatively divided into three cases. At relatively large V, ε changes little over a wide range of impact velocity. Below $V \approx 0.25$ cm^{-1},

ε increases rapidly with decreasing V. The extrapolation of our data indicates that, at a sufficiently small but finite velocity, ε approaches unity. This behaviour at the low velocity limit is consistent with the classical theory of nearly elastic deformation associated with low-velocity impacts[16–18]. However, the asymptotic plateau for relatively large velocity cannot be accounted for by any existing collision model.

The data presented in Fig. 1 can be fitted remarkably well with a power law

$$\varepsilon = (0.32 \pm 0.02)\, V^{-0.234 \pm 0.008} \quad (2)$$

where V is the impact velocity measured in cm s^{-1} for the range $0.015 < V < 5.1$. Extrapolation of this power law indicates that $\varepsilon \to 1$ for $V < V_c = 0.008$ cm s^{-1}. The dispersion of the data, relative to the best fitted curve, is much larger for intermediate collision velocities than for large velocities, where ε attains an asymptotic value of 0.25, and for very small velocities where ε approaches unity. Special care has been taken to eliminate various possible external causes for this large dispersion. A trial experiment for collision between a solid synthetic rubber ball (super ball) and a rigid surface yielded an ε–V relationship with dispersion of order less than one-tenth those found for ice ball-block collisions. Clearly, the scattering of the data is considerably larger than the typical measurement uncertainty which is indicated in Fig. 1. We propose that the large dispersion in the data is real, and is probably associated with compression and random powdering of tiny ice chips on the surface. Irregularities in the shape of the ice chips can lead to considerable variation in the radius of curvature and geometry of the contacting surfaces of the ice ball and block. The tendency for the dispersion to decrease at relatively large impact velocities is probably caused by the surface distortion during a collision being large enough to override any variation in the surface geometry immediately before each collision.

Note that the effective mass involved in a collision is 5.4 times larger than the mass of the ice ball mounted to the pendulum. Because the ice block is held stationary, it has an infinite inertial mass. In any event, as Saturn's rings are composed of ice particles with a large range in size, it is desirable to investigate collisions between particles with various masses and sizes. These investigations are underway and the results will be presented elsewhere.

Despite recent considerable observational and theoretical advances in our understanding of Saturn's rings, the actual physical nature of the constituent particles remains unclear. The rings may either be made of solid particles with relatively smooth surface radius of curvature or particles covered with loose ice chips[19]. The amount of gas and dust inclusions in the ring particles is also unknown. In our experiments, both the ice ball and ice block are prepared with a smooth surface and are relatively free of gas or dust. (The amount of surface frost on the ice ball has also been minimized although this can never be eliminated.) Furthermore our data are obtained for direct collisions whereas grazing collisions may be far more common in Saturn's rings. Thus, it is not entirely clear to what extent the data obtained from the above experiment are relevant to the structure of Saturn's rings. Nonetheless, we apply our results to the standard uniform-size hard sphere model[8] for simplicity. Under this assumption, V_c defines a lower limit on the thickness of the disk which is $\sim V_c/\Omega = 50(V_c/0.01\ \text{cm s}^{-1})(10^{10}\ \text{cm}/r)^{3/2}$ cm. If we apply the results of equation (2) to equation (1), it follows that

$$H = 2f\sigma/\Omega = 80f[1 - b/(1+\tau^2)]^{-2.1}(r/10^{10}\ \text{cm})^{3/2}\ \text{cm} \quad (3)$$

Applying an idealized, uniform-particle sized model, we derive for most regions of the ring that $H < 5$ m, provided the particle size is smaller than H. This value is consistent with that deduced from microwave scattering experiments[2]. The slight difference between these values and those deduced from resonant damping analyses[3] may be due to the additional energy source associated with external perturbers.

In the absence of external stimulation, such as Saturn's satellite resonances, the energy equilibrium implies an effective viscosity

$$Nu \approx 0.3(r/10^{10}\ \text{cm})^{3/2}\frac{[1 - b/(1+\tau^2)]^{-4.2}}{(\tau + \tau^{-1})}\ \text{cm}^2\ \text{s}^{-1} \quad (4)$$

and a corresponding diffusion time $T_d \simeq r^2/v$, longer than the age of the Solar System. The corresponding viscous stress is plotted in Fig. 2. Superimposed on the actual data is a W–τ relationship derived from equation (2) such that

$$W \sim [1 - b/(1+\tau^2)]^{-4.2}\tau^2/(1+\tau^2) \quad (5)$$

The maximum value of W is attained at $\tau_c = (1-b)/(4.2b-1)$. The scatter of the original data (Fig. 1) is amplified in Fig. 2 by numerous mathematical transformations of the experimental data. The results in equation (5) imply that, for $\tau \gtrsim 0.5$, W decreases with τ and therefore the rings are unstable. For $\tau \lesssim 0.5$, the rings are stable. If we were to take the widely scattered data points, the critical τ would lie in the range 0.3–0.7. Thus, the optically thick regions of the disk are expected to be diffusionally unstable and would open up low density regions with τ of the order 0.5–0.7. The observed optical depth profile of the B ring indicates that the typical τ in the less opaque regions of the B ring is ~0.6 (ref. 3).

In the above discussion we have not considered the effect of particle size distribution. Note that the large, metre-size particles have radii comparable to or larger than the ring thickness, as derived from equation (3), such that they may form a 'monolayer'. For these particles the velocity dispersion is determined by the gradient of the rings' keplerian velocity across their diameter[7] so that their W monotonically increases with τ and their motion is viscously stable. Consequently, the small centimetre-size particles and the large metre-size particles in the high τ B ring may have rather different radial structure. Voyager's data indicate that the primary contribution to the τ variation in the B ring is from the small particles. The large particles have a relatively smooth radial distribution. Thus, a realistic model for the evolution of the B ring requires a detailed analysis of the collisionally induced transport process for a collection of particles with different sizes (G. Stewart, in preparation). We intend to supplement the experimental data presented here with data on collisions between ice balls with different radii of curvature at the contact point.

The above results may also be applied to study the actual damping process in resonant excited density waves[20,21], the structure of narrow rings and sharp edges as well as the satellite shepherding phenomenon[22]. As for our experiments, variations in ice ball's and ice block's surface geometry, surface crystal lattice structure, collisional grazing angles, and ambient temperature will be examined in future. In general, we believe that the results presented here are a first step towards understanding ice-particle collisional processes.

We thank Drs N. Borderies, P. Goldreich, J. Papaloizou, E. Stone and S. Tremaine for useful conversations. This work is partially supported by NSF grants AST-81-00163, DMR-82-05421 and a grant from the California Space Institute CS10-83. Lick Observatory contribution no. 435.

Received 14 December 1983; accepted 13 March 1984.

1. Lane, A. L. *et al. Science* **215,** 537–543 (1982).
2. Zebker, H. A. & Tyler, G. L. *Science* (in the press).
3. Esposito, L. W., O'Callaghan, M. & West, R. A. *J. geophys. Res.* **88,** 8643–8649 (1983).
4. Marouf, E. A., Tyler, G. L., Zebker, H. A., Simpson, R. A. & Eshleman, V. R. *Icarus* **54,** 189–211 (1983).
5. Smith, B. A. *et al. Science* **215,** 504–537 (1982).
6. Cook, A. F. & Franklin, F. A. *Astr. J.* **69,** 173–200 (1964).
7. Brahic, A. *Astr. Astrophys.* **54,** 895–907 (1977).
8. Goldreich, P. & Tremaine, S. *Icarus* **34,** 227–239 (1978).
9. Hameen-Antilla, K. A. & Lukkari, J. *Astrophys. Space Sci.* **71,** 475–497 (1980).
10. Lynden-Bell, D. & Pringle, J. *Mon. Not. R. astr. Soc.* **168,** 603–637 (1974).
11. Goldsmith, W. *Impact* (Arnold, London, 1960).
12. Hameen-Antilla, K. A. *Astrophys. Space Sci.* **58,** 477–519 (1978).
13. Ward, W. R. *Geophys. Res. Lett.* **8,** 641–643 (1981).
14. Lukkari, J. *Nature* **292,** 433–435, (1981).
15. Lin, D. N. C. & Bodenheimer, P. *Astrophys. J. Lett.* **248,** L83–L86 (1981).
16. Andrew, J. P. *Phil. Mag.* **9,** 593–610 (1930).
17. Landau, L. & Lifshitz, E. M. *Theory of Elasticity* (Pergamon, London, 1959).
18. Borderies, N., Goldreich, P. & Tremaine, S. in *Planetary Rings* (eds Greenberg, R. & Brahic, A.) (University of Arizona, in the press).
19. Weidenschilling, S. J., Chapman, C. R., Davis, D. R. & Greenberg, R. in *Planetary Rings* (eds Greenberg, R. & Brahic, A.) (University of Arizona, in the press).
20. Lissauer, J. J., Shu, F. H. & Cuzzi, J. N. *Proc. IAU Colloq.* **75,** (in the press).
21. Shu, F. H., Cuzzi, J. N. & Lissauer, J. J. *Icarus* **53,** 185–206 (1983).
22. Borderies, N., Goldreich, P. & Tremaine, S. *Nature* **299,** 209–211 (1983).